Journal of Alloys and Compounds 566 (2013) 83–89

Contents lists available at SciVerse ScienceDirect

Journal of Alloys and Compounds

journal homepage: www.elsevier.com/locate/jalcom

Structural and optical properties of Zn–In–Te thin films deposited by thermal evaporation technique

H.H. Güllü [a], Ö. Bayraklı [a], İ. Candan [a], E. Coşkun [a,b], M. Parlak [a,*]

[a] Department of Physics, Middle East Technical University, GUNAM, 06800 Ankara, Turkey
[b] Department of Physics, Çanakkale Onsekiz Mart University, 17100 Çanakkale, Turkey

ARTICLE INFO

Article history:
Received 7 January 2013
Received in revised form 1 March 2013
Accepted 9 March 2013
Available online 19 March 2013

Keywords:
Thin films
Optical properties
Crystal structure
Optical spectroscopy
X-ray diffraction

ABSTRACT

Annealing effects on structural and optical properties of the thermally evaporated Zn–In–Te (ZIT) thin films have been investigated. The structural and the compositional analyses were carried out by means of X-ray diffraction (XRD) and energy dispersive X-ray analysis (EDXA). The as-grown and annealed ZIT films had polycrystalline structure and the preferred orientation changed from (220) to (112) direction with increasing annealing temperature. The optical properties and constants were determined by transmittance measurements in the wavelength range of 200–2000 nm. The effect of annealing on the optical parameters was determined by using Single Oscillator Model (SOM), Envelope Model (EM) and Cauchy Method. The absorbance studies revealed that the films had three distinct transitions in the high absorption region because of the tetragonal distortion, and that was used to evaluate the splitting energies of crystal-field and spin–orbit splitting. The fundamental optical band gap values were found to be lying in the range of 1.51 and 1.72 eV and the notable change of the band gaps due to annealing temperatures was observed. Finally, the Urbach energies were calculated and it was observed that the band tail energies were increasing with increasing annealing temperature.

1. Introduction

In recent years, the polycrystalline ternary II–III–VI_2 (i.e. $CuInSe_2$, $Cu(In,Ga)Se_2$, $CdGa_2Te_4$, $ZnGa_2S_4$, $ZnIn_2Te_4$) and their binary analogies from II–VI (i.e. CdTe, ZnSe, ZnTe) semiconductor compounds have been extensively studied because of their potential applications, particularly, in the area of thin film solar cells and also large area electronic devices such as field effect transistors, radiation detector, optical thin film filters, nonlinear integrated optical devices, light emitting diodes (LEDs) and laser heterostructure for emission in the infrared spectral range [1,2]. Their interesting and fascinating electrical and optical properties, especially easy tunable band gap values and having high absorption coefficients, make them a candidate for absorbing layer in the fabrication of thin film solar cell [3].

In order to find a powerful candidate for desired optoelectronic device applications, the basic studies about the structural and the optical properties of the materials are very important to investigate crystallinity, energy band gap, refractive index and dielectric constants. Some studies have revealed that ZnTe and $ZnIn_2Te_4$ can be suitable compounds due to their direct band gap values of 2.26 eV [4,5] and among 1.40–1.90 eV [6–9], respectively.

In this work, the ternary compound Zn–In–Te (ZIT) has been studied for the possible usages in the optoelectronic and photovoltaic device applications. The results of the systematic studies were carried out to investigate the effects of post-annealing on the structural and optical properties of the films deposited on glass substrates by the thermal evaporation of the sintered crystal powder under the high vacuum. The annealing processes were applied to the grown films in between 300 and 500 °C under nitrogen atmosphere.

2. Experimental details

In this study, ZIT thin films were deposited onto well-cleaned soda lime glass substrate by thermal evaporation method by using the stoichiometric polycrystalline powder under vacuum of 10^{-6} Torr. The evaporation powder was prepared using mixture of Zinc (Zn), Indium (In) and Tellurium (Te) with 99.999% purity (from Alfa-Easer, US). The constituent elements were weighted in 1:1:2M ratios and placed in chemically cleaned quartz ampoule and sealed in vacuum of 10^{-5} Torr. Following to this process, the quartz ampoule was placed in a specially designed vertical Lindberg Furnace, and then heated up slowly with the temperature rate of 100 °C/h to 1150 °C, oscillation process was applied for 6 h to provide uniform mixture of constituent elements and kept at this temperature for another 12 h. Then, the same heating rate was applied during the cooling. After sintering process, the sintered crystal was taken out by cutting the quartz ampoule. For the evaporation cycle, the substrate holder was mounted almost 15 cm above the source in the evaporation chamber. During deposition under vacuum of about 10^{-6} Torr, the substrate temperature was kept at constant temperature of about 250 °C. The evaporation rate was arranged to ~6.00 Å/s and monitored with a quartz crystal by Inficon XTM/2 thickness monitor. The thicknesses of the as-grown

* Corresponding author. Tel.: +90 312 2107646; fax: +90 312 2105099.
E-mail address: parlak@metu.edu.tr (M. Parlak).

0925-8388/$ - see front matter © 2013 Elsevier B.V. All rights reserved.
http://dx.doi.org/10.1016/j.jallcom.2013.03.030

films were also measured electromechanically by Dektak 3030ST profilometer. Following to the deposition, the post annealing procedure was applied in the temperature range of 300–500 °C by 100 °C step for 30 min under nitrogen atmosphere. The X-ray diffraction (XRD) measurements were performed by using Rigaku Miniflex XRD system equipped with Cu Kα radiation source with the wavelength of 1.54 Å. The structural analysis together with peak matching was made by using the computer software and ICDD database. A JSM-6400 scanning electron microscope (SEM) equipped with energy dispersive X-ray analysis (EDXA) detector facility operated at 20 kV was used to determine the chemical composition of the powder and the thin film samples. Finally, the spectral optical transmittance measurements were carried out by using a Lambda 950 UV/Vis/NIR spectrophotometer in the wavelength range of 200–2000 nm.

3. Results and discussion

3.1. Structural analysis

The composition of constituent elements of the deposited thin films and the source powder were determined by using EDXA. The atomic weight percentages of the constituent elements in the powder and deposited films were measured and listed in Table 1 with annealing temperatures. As observed from Table 1, there are significant fluctuations in the elemental compositions of the deposited films and the source crystal powder. Particularly, it indicates that when the atomic percentage of Zn and Te increased with annealing at 300 °C, the atomic percentage of In in the samples decreased. For the film annealed at 400 °C, the atomic percentages of In and Te showed small increasing behavior, as Zn was decreasing. When the film was annealed at 500 °C, the variation of Te content in the structure had more pronounced effect with a decrease as compared with other annealing temperatures and the contents of Zn and In increased. The analyses showed that the as-grown films had indium deficient, Zn and Te rich compositions. On the other hand, no systematic decrease or increase was observed in the compositions of the annealed films. Therefore, these differences in the EDXA results of the source and deposited films can be explained in terms of the different vapor pressures of the constituent elements ($P_{In} > P_{Te} > P_{Zn}$). That results in the segregation and re-evaporation of the constituent elements. This fluctuation can yield the variation in the structural formation because of the solubility of the constituent elements within this ternary structure [10]. XRD patterns of as-grown and annealed ZIT films are given in Fig. 1 together with the crystal powder. As seen from the figure, the XRD analysis showed that sintered ZIT powder had polycrystalline tetragonal structure having the lattice constants $a = 6.119$, $b = 6.119$ and $c = 12.257$ Å with the main diffraction peaks along (220), (228) and (316) directions. Also, ZIT thin film samples deposited at the substrate temperature of 250 °C showed a polycrystalline structure whether they were annealed or not. It was observed that the diffraction intensity along the (220) direction increased sharply with increasing the annealing temperature up to 300 °C. However, after 300 °C annealing, there was a change in the main orientation from (220) to (112) direction for the films annealed at 400 °C, which could be taken as the beginning of phase change in the structure of the films. This can be the verification of the compositional changes for the 400 °C annealed samples as observed from EDXA results. As seen from Fig. 1, for the sample annealed at 500 °C, the main orientation direction was found to be along (112) direction that shows the structural modification by giving thermal energy to change and/or to complete the structural properties. According to Müller et al. [11], comparison of the degree of preferred orientation in the samples was done in terms of the texture parameter R_I from the ratio of diffraction peak intensities in the XRD pattern. The variable R_I values were calculated using the relation;

$$R_I = \frac{I_{hkl}}{\sum_{all\ peaks} I_{hkl}}, \tag{1}$$

in which (hkl) represents the diffraction peak intensity of (220) plane for as-grown and the 300 °C annealed film, and the intensity of (112) plane for the films annealed at 400 and 500 °C. $\sum I_{hkl}$ represents the overall summation of all diffraction peak intensities seen in XRD scan. The calculated values listed in Table 2 showed that R_I values for (220) are decreasing, but for (112) are increasing with increasing annealing temperature, which implies that the texture of film structure changes with annealing temperature except the values for 300 °C annealed samples. Most probably, that can be explained with the changes in the stoichometry of the films. This is in good agreement with the result obtained from the compositional analysis.

The average grain size D was estimated from the XRD pattern using the Scherrer's formula [12] and expressed as;

$$D = \frac{K\lambda_0}{\beta \cos\theta}, \tag{2}$$

where λ_o is the wavelength of X-ray radiation source, β is the full width half maximum value of a diffraction peak, θ is the diffraction angle, and K is the Scherrer's constant in the order of unity for usual crystal structure and in this study due to cubic symmetry, K was taken as about 0.94 [12]. The calculated D values depending on annealing temperatures were listed in Table 2. The increase in grain

Table 1
EDXA results for as-grown and annealed ZIT films.

Sample	Zn at.%	In at.%	Te at.%
Crystal	16.81	39.76	43.43
As-grown	30.83	16.81	52.36
A 300	31.92	14.73	53.35
A 400	30.63	15.67	53.69
A 500	32.67	17.05	50.00

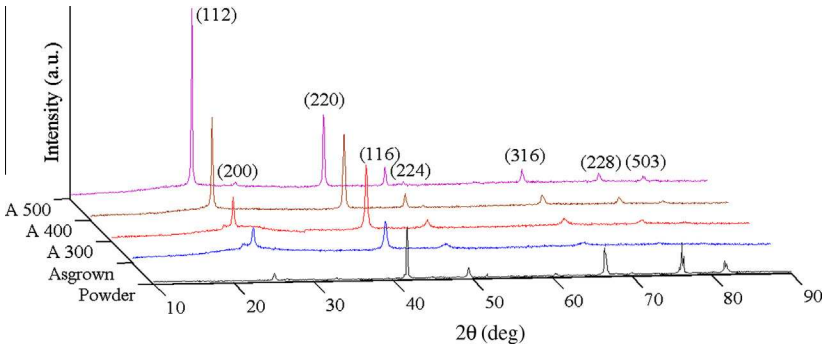

Fig. 1. XRD diffractograms for crystal powder, as-grown and annealed ZIT films at 300, 400 and 500 °C.

Table 2
Texture parameter R_I values for (220) and (112) planes, and D values for as-grown and annealed ZIT films.

Sample	R_I (220)	R_I (112)	D (nm)
As grown	0.46	0.39	21.5
A 300	0.83	0.37	30.2
A 400	0.50	0.69	25.2
A 500	0.29	1.11	28.9

size with the annealing can be referred as the indication of improvement in the crystallinity.

3.2. Optical analysis

In order to understand the optical properties of ZIT thin films optical constants, such as, absorption coefficient, band gaps, refractive index, and dielectric constants. must be determined by using the spectral transmittance measurement that is a simple tool to obtain these constants. Transmittance spectra of the as-grown and annealed ZIT films at different temperatures in the wavelength range of 200–2000 nm at room temperature were measured and shown in Fig. 2. Transmittance values ($T(\lambda)$) of all films in the spectral range of 850–2000 nm were around 80%. $T(\lambda)$ values decreased when the samples annealed at 500 °C, but the transmittance values for as-grown and annealed films at 300 °C and 400 °C were almost close to each others. The remarkable decrease of $T(\lambda)$ values for the film annealed at 500 °C could be explained with the change in the structural and surface behaviors due to the variations in the stoichometry of the film structure as observed from EDXA results (see Table 1). Once the ratios of Zn and In rise, the metallic property of the film was more effective, therefore the surface of the film became more reflective.

The complex refractive index, $\widehat{n}$ is expressed as;

$$\widehat{n}(\lambda) = n(\lambda) - i\kappa(\lambda), \tag{3}$$

where $n(\lambda)$ is the real part of the refractive index and $\kappa(\lambda)$ is the extinction coefficient for the films as a function of incident light wavelength (λ). $n(\lambda)$ values of the as-grown and annealed samples were calculated by using the envelope method developed by Swanepoel [13]. By the help of EM, $n(\lambda)$ values can be calculated by using the relation;

$$n = \left[N + \left(N^2 + n_s^2 n_o^2\right)^{1/2}\right]^{1/2}, \tag{4}$$

and N can be written as;

$$N = \frac{n_o^2 + n_s^2}{2} + 2n_s n_o \frac{T_M - T_m}{T_M T_m}, \tag{5}$$

here n_o is the refractive index of the air which is equal to $n_o = 1$, T_{max} and T_{min} are the maximum and minimum values of envelope curves of transmittance, n_S is the refractive index of the substrate that was obtained through the following relation;

$$n_s = \frac{1}{T_S} + \left(\frac{1}{T_S^2} - 1\right), \tag{6}$$

where T_S is the maximum value of $T(\lambda)$. $n(\lambda)$ values were calculated in between 800–2000 nm for the as-grown and annealed films and plotted in Fig. 3. This wavelength region could be expressed as the weak absorption and transparent region according EM [13]. The calculated $n(\lambda)$ values were also fitted by three-term Cauchy relation which is expressed as,

$$n(\lambda) = A + \frac{B}{\lambda^2} + \frac{C}{\lambda^4}, \tag{7}$$

and evaluated Cauchy parameters (A, B, C) are given in Table 3. It is obvious that, there is a sharp increase in $n(\lambda)$ values for the film annealed at 500 °C because of the changes in the film structure as observed from XRD and EDXA analyses. In order to check and to be sure about the consistency of the applied envelope method, mechanically measured film thicknesses were compared with the calculated ones from the EM by using following relation,

$$d_{EM} = \frac{\lambda_1 \lambda_2}{2(\lambda_1 n_2 - \lambda_2 n_1)}. \tag{8}$$

here n_1 and n_2 are the refractive index of two adjacent $T(\lambda)$ maxima or minima of the interference fringes located at λ_1 and λ_2, respectively. The measured and calculated thicknesses of the films (namely, d and d_{EM}) are given in Table 3. d_{EM} values are found to be in good agreement with the measured d values. And then the other optical parameter, extinction coefficient $\kappa(\lambda)$ of the samples was calculated from expression [14],

$$\kappa(\lambda) = \frac{\lambda}{4\pi}\alpha(\lambda), \tag{9}$$

where $\alpha(\lambda)$ is the absorption coefficient and can be determined by using the equation,

$$\alpha(\lambda) = -\frac{1}{d}\ln\left(\frac{1}{T(\lambda)}\right). \tag{10}$$

The calculated $\kappa(\lambda)$ values were plotted in Fig. 4. As seen from the figure, $\kappa(\lambda)$ values for annealed at 500 °C increases depending on the rising of the atomic ratios of Zn and In atoms which causes more metallic behavior on the surface and there is no remarkable change in $\kappa(\lambda)$ values for as-grown and annealed at 300 and 400 °C as expected from EDXA results. The relation between the $\widehat{n}(\lambda)$ and dielectric dispersion $\varepsilon(\lambda)$ can be written as [14],

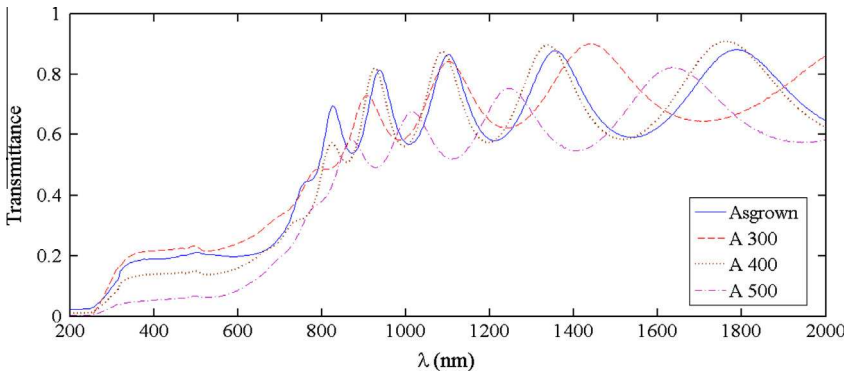

Fig. 2. The transmittance spectrum of the as-grown and annealed ZIT films at 300, 400 and 500 °C.

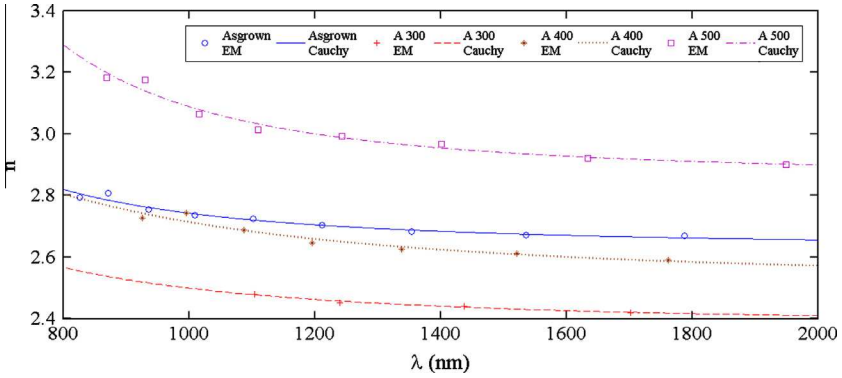

Fig. 3. The calculated refractive index values by EM and by three term Cauchy Parameters for as-grown and annealed ZIT films at 300, 400 and 500 °C.

Table 3
Three term Cauchy Parameters, the measured and calculated thickness values, and SOM model parameters for as-grown and annealed ZIT films.

Sample	Cauchy parameters			Thickness (nm)		E_p (eV)	E_d (meV)	ε_0	ε_∞	n_0
	A	B (nm^2)	C (nm^4)	Dektak	Env.					
Asg	2.63	9.39×10^4	1.82×10^{10}	1040 ± 1	1046 ± 1	4.05	23.95	4.91	7.76	2.22
A 300	2.38	1.20×10^5	6.21×10^6	965 ± 1	961 ± 1	3.69	17.23	3.67	6.44	1.92
A 400	2.52	2.13×10^5	-1.92×10^{10}	990 ± 1	992 ± 1	3.06	16.50	4.39	7.66	2.10
A 500	2.86	1.50×10^5	8.12×10^{10}	981 ± 1	976 ± 1	3.11	22.12	6.11	10.22	2.47

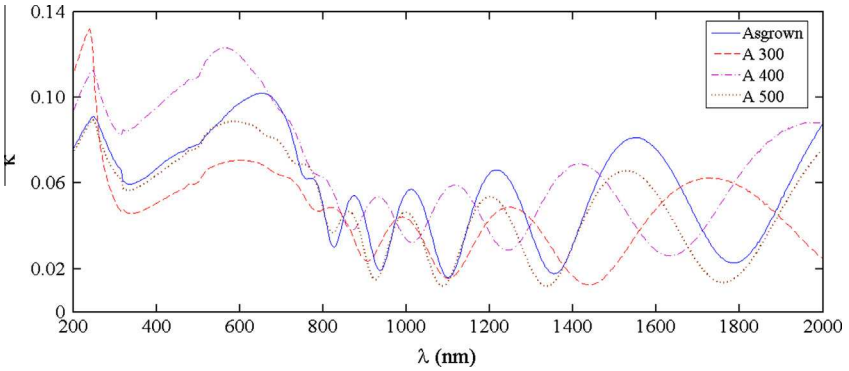

Fig. 4. The determined extinction coefficient values for the as-grown and annealed ZIT films at 300, 400 and 500 °C.

$$\widehat{n}(\lambda) = [\varepsilon(\lambda)]^{1/2} = [\varepsilon_{re}(\lambda) + i\varepsilon_{im}(\lambda)]^{1/2}, \tag{11}$$

where $\varepsilon_{re}(\lambda)$ and $\varepsilon_{im}(\lambda)$ are real and imaginary part of $\varepsilon(\lambda)$, respectively, and they can be expressed as,

$$\varepsilon_{re}(\lambda) = n(\lambda)^2 + \kappa(\lambda)^2, \tag{12}$$

and

$$\varepsilon_{im}(\lambda) = 2n(\lambda)\kappa(\lambda). \tag{13}$$

The calculated $\kappa(\lambda)$ values were very small as compared with $n(\lambda)$ values (see Figs. 3 and 4). Then $\varepsilon_{re}(\lambda)$ is approximately equal to $n^2(\lambda)$ and also $\varepsilon_{im}(\lambda)$ is closed to $2\kappa(\lambda)$. Therefore, the dielectric constants could be rewritten as,

$$\varepsilon_{re}(\lambda) \cong n^2(\lambda), \tag{14}$$

$$\varepsilon_{im}(\lambda) \cong 2\kappa(\lambda). \tag{15}$$

The obtained $\varepsilon_{re}(\lambda)$ values from Eq. (14) were plotted in Fig. 5. As observed from the figure, annealing the films at 300 °C resulted in a decreasing dielectric constant, but further annealing produced increasing behavior of the dielectric constant. This increasing behavior together with increasing refractive index may refer to the improvement in the crystallinity of the films as observed from XRD analyses. The determination of the refractive index by Cauchy equation made it possible to use for Single Oscillator Model (SOM) which can be defined as,

$$n^2 - 1 = \frac{E_p E_d}{E_p^2 - (h\upsilon)^2}, \tag{16}$$

where E_d is a parameter which gives a measure of the strength of the interband optical transitions, E_p is a parameter which gives the average energy gap also called oscillatory energy, h is Planck constant and υ is frequency [15]. The SOM parameters E_d and E_p were calculated from the linear part of $(n^2 - 1)^{-1}$ versus $(h\nu)^2$ plot at low energy values for as-grown and annealed ZIT films as shown in Fig. 6. By the SOM model, the static dielectric constant (ε_0) and static refractive index (n_0) could be determined from the intercept and the slope of the plots by using E_d and E_p values. ε_0 approaches the real part of the $\varepsilon(\lambda)$ value below the Reststrahlen range in optical spectra [14] and n_0 is the real refractive index via ε_0 value. The optical constant connecting the Reststrahlen-near-infrared range is called the high frequency dielectric constant ε_∞ [14]. ε_∞ values for the studied film were calculated from Fig. 5 at λ = 830 nm which is just below the minimum absorption edge (see Fig. 7). The calculated

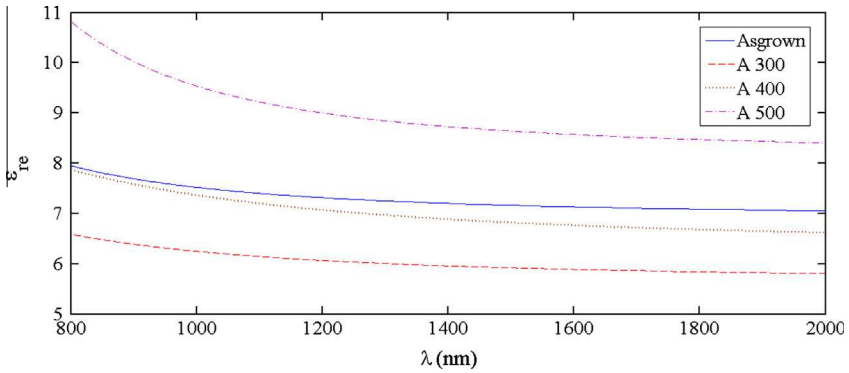

Fig. 5. The real part of dielectric dispersion for the as-grown and annealed ZIT films at 300, 400 and 500 °C.

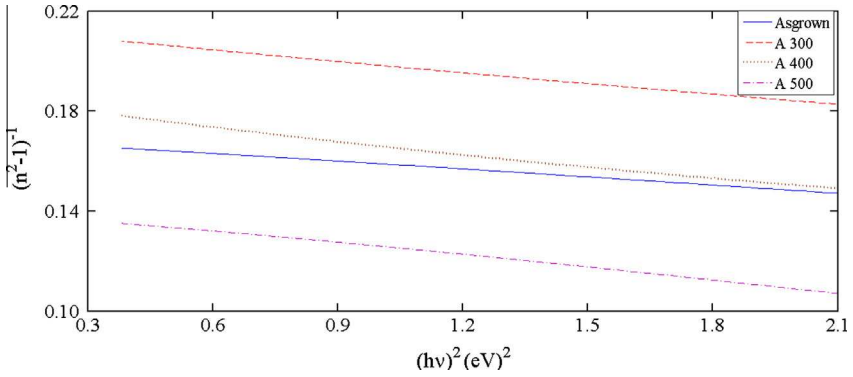

Fig. 6. Plots of $(n^2-1)^{-1}$ versus $(h\upsilon)^2$ for the as-grown and annealed ZIT films at 300, 400 and 500 °C.

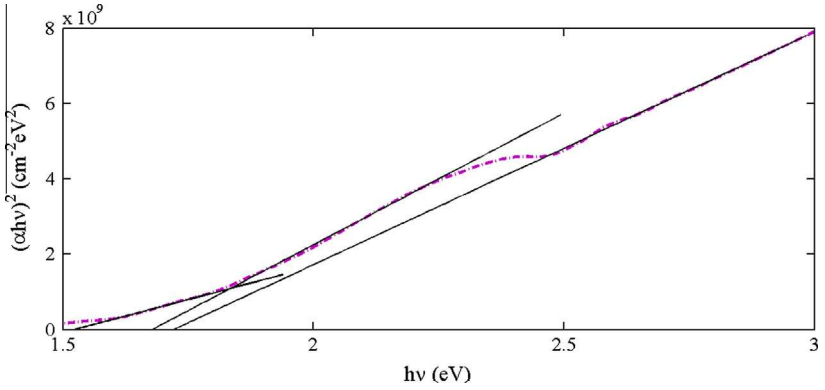

Fig. 7. Typical plot of $(\alpha h\upsilon)^2$ versus $(h\upsilon)$ for the films annealed at 500 °C. The straight lines show the linear parts of the plot for each transition.

E_p, E_d, ε_0, n_0 and ε_∞ values for the studied films were listed in Table 3. ε_0 and ε_∞ constants are also related to long-wavelength transverse optical and longitudinal optical phonon frequencies by well-known Lyddane–Sachs–Teller relation [16] which gives the information about the amount of the polar character in the chemical bonds of these compounds [14]. Also, it is noted that $\varepsilon_o \sim \varepsilon_\infty$ and $\varepsilon_o > \varepsilon_\infty$ represent for homopolar and heteropolar crystal structures, respectively [14]. As a result of analyses on the ZIT samples, it was observed that they had hetero-polar crystal structure (see Table 3).

The other important parameter in semiconductor materials is the optical band gap (E_g) values and they can be calculated by means of absorption coefficient. In general, absorption spectra of the materials can be divided into three principle regions according to the work of Wood and Tauc [17]. They are named as the strong absorption region (where $\alpha > 10^4$ cm^{-1}), the Urbach region (where $10^4 > \alpha > 1$ cm^{-1}) and very low absorption region (where $\alpha < 1$ cm^{-1}). In the strong absorption region, $(\alpha h\upsilon)$ could be described by the relation

$$(\alpha h\nu) = A(h\nu - E_g)^m, \tag{17}$$

Table 4
Band gap values, quasicubic model parameters and band tail energy values for as-grown and annealed ZIT films.

Sample	E_{g1} (eV)	E_{g2} (eV)	E_{g3} (eV)	$-\Delta_{CF}$ (eV)	Δ_{SO} (eV)	E_U (eV)
As grown	1.51	1.53	1.72	0.026	0.205	0.084
A 300	1.51	1.53	1.61	0.019	0.083	0.103
A 400	1.50	1.56	1.56	0.037	0.026	0.116
A 500	1.52	1.68	1.72	0.186	0.030	0.146

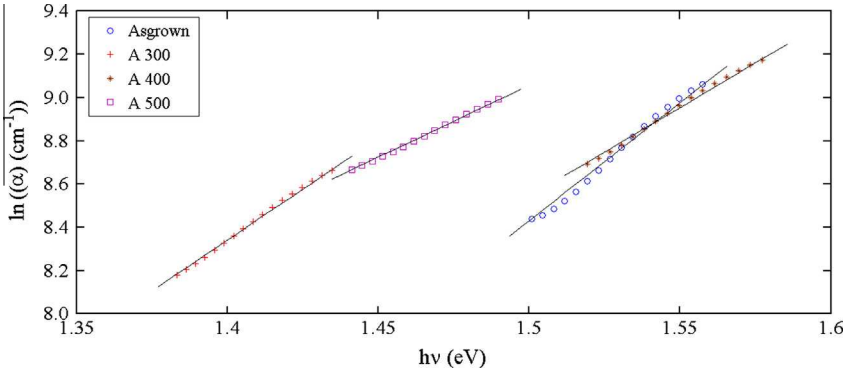

Fig. 8. Typical plots of $\ln(\alpha)$ versus $(h\upsilon)$ for as-grown and annealed ZIT films at 300, 400 and 500 °C. The black lines show the linear parts of the plots for band tail energies.

where A is an energy-independent constant and E_g is the optical band gap. The exponent m depends on the nature of the electronic transition responsible for the absorption, $m = 1/2$, 2, 3/2 or 3 for allowed direct, allowed indirect, forbidden direct or forbidden indirect transitions, respectively [18]. For allowed direct transition ($m = 1/2$), the $(\alpha h\upsilon)^2$ versus $(h\upsilon)$ variations for as-grown and annealed films at 300, 400, and 500 °C were plotted as seen in Fig. 7 for typical sample and E_g values were calculated using the extrapolation on the energy axis of $(\alpha h\upsilon)^2$ versus $(h\upsilon)$ plots for the studied films (see Table 4). The non-linear steps in the high absorption region can be attributed to the absorption related with the impurity states or interference effects due to multiple reflections occurring at the surface and backside of the film [11]. However, in these samples because of non-stoichiometry as observed from EDXA results, any secondary phase was not observed, then it was concluded that these transitions obtained from the variations of absorption coefficient most probably related with band to band transitions due to the splitting of the valance band into three bands due to d-like valance band states and p-like conduction band states [19,20]. This might be the result of tetragonal distortion and then the quasi-cubic model could be used to obtain the crystal-field splitting (Δ_{CF}) and spin–orbit splitting (Δ_{SO}) [19] by using the relation,

$$E_{1,2} = -\frac{1}{2}(\Delta_{cf} + \Delta_{so}) \pm \frac{1}{2}\left[(\Delta_{cf} + \Delta_{so})^2 - \frac{8}{3}(\Delta_{cf}\Delta_{so})\right]^{1/2}, \quad (18)$$

where, $E_{1,2}$ are defined as the energy differences of $E_1 = E_{g2} - E_{g1}$ and $E_2 = E_{g3} - E_{g2}$. The calculated values of Δ_{cf} and Δ_{so} are given in Table 4. It was observed that Δ_{so} decreased as Δ_{cf} was increasing (except the annealing at 300 °C) with increasing annealing temperature. This can be related with structural changes and modifications (with annealing process) as observed from the structural analysis. Furthermore, the Urbach tail region corresponds to absorption involving one or both of the band tails with additional broadening expected from any fluctuations arising from charged defect states and lattice vibrations [14]. The Urbach energy (E_U) indicates the width of the tail states and can be determined by using the expression [14],

$$\alpha = \alpha_o \exp\left(\frac{h\nu - E_g}{E_U}\right), \quad (19)$$

where α_o is a constant. As seen from Fig. 8, the semi logarithmic plots of (α) as a function of $(h\upsilon)$ were used to calculate Urbach energies for the as-grown and the annealed films, and the calculated values for the linear regions are given in Table 4. E_U values increased with increasing annealing temperature for ZIT films because of the changing of the atomic percentages of alloys, which could cause to increase the band tail states. Calculated E_{g3} values can be accepted as the main band-to-band transition because of having the longest linearity for the fundamental absorption edge, and decreasing via increasing annealing temperature due to the rising E_U values except for the film annealed at 500 °C. The structural analyses indicate that there is a structural chance depending on annealing temperature and this could be the reason of the increasing E_{g3}.

4. Conclusion

In this work the structural and optical properties of thermally evaporated ZIT thin films were investigated depending on annealing temperatures in between 300 and 500 °C. X-ray studies showed that the preferred orientation was along the (220) direction for the as-grown and the annealed films at 300 and 400 °C, however, for the film annealed at 500 °C it chanced from (220) to (112) direction. The EDXA analysis revealed that the Zn and In ratios of the film annealed at 500 °C increased remarkably. The changes in the compositions of the samples with annealing resulted in the fluctuation in the film structure and gave rise to the structural defects. The optical analysis of ZIT films was studied by measuring the transmittance spectra in the wavelength range of 200–2000 nm. The thermal annealing process produced the pronounced effects on the refractive index, extinction coefficient and the SOM parameters of the ZIT films. The analysis of $(\alpha h\upsilon)^2$ versus $(h\upsilon)$ plots showed that there were three different transitions in the optical band regions of ZIT films. The fundamental band gap values (E_{g3}) were calculated as 1.72, 1.61, 1.56 and 1.72 eV for as-grown and films annealed at 300, 400 and 500 °C, respectively. The remarkable change of E_{g3} values with respect to annealing temperatures could be a significant property for the device application of ZIT films. The band-to-band transitions depending on annealing temperature were analyzed and the hybridization of the splitting of d-like valance band states and p-like conduction band states were determined. Finally, the Urbach energies calculated from the Urbach tail regions showed increasing behavior with increasing annealing temperature. That may also be taken as the modification in the structure of the films, and resulted in different trap levels related with the surface and the bulk properties of ZIT films.

Acknowledgements

This work was financed by Middle East Technical University (METU-BAP) under Grant No. BAP-01-05-2012-004. Also, one of the authors would like to thank to TUBITAK-BIDEB for the financial supports during this study.

References

[1] S. Ozaki, K. Muto, H. Nagata, S. Adachi, J. Appl. Phys. 97 (2005) 043507–043511.
[2] A.K.S. Aqili, A.J. Saleh, Z. Ali, S. Al-Omari, J. Alloys Comp. 520 (2012) 83–88.
[3] V. Alberts, Mater. Sci. Eng. B – Adv. 107 (2004) 139–147.
[4] S. Ozaki, S. Boku, S. Adachi, Phys. Rev. B 68 (2003) 235201–235211.

[5] A. Erlacher, A.R. Lukaszew, H. Jaeger, B. Ullrich, Surf. Sci. 600 (2006) 3762–3765.
[6] L. Feng, L. Wu, Z. Lei, W. Li, Y. Cai, W. Cai, J. Zhang, Q. Luo, B. Li, J. Zheng, Thin Solid Films 515 (2007) 5792–5797.
[7] P. Manca, F. Raga, A. Spiga, Phys. Status Solidi A 16 (1973) K105–K108.
[8] S. Ozaki, S. Adachi, Phys. Rev. B 64 (2001) 085208–085211.
[9] P. Manca, F. Raga, A. Spiga, Nuovo Cimento Soc. Ital. Fis., B 19 (1974) 15–28.
[10] C.L. Yaws, Handbook of Vapor Pressure, vol. 4, first ed., Inorganic Compounds and Elements, Golf Publishing Company, Houston, Texas, 1995.
[11] J. Muller, J. Nowoczin, H. Schmitt, Thin Solid Films 496 (2006) 364.
[12] J.I. Langford, A.J.C. Willson, A. Survey, J. Appl. Cryst. 11 (1978) 102.
[13] R. Swanepoel, J. Phys. E: Sci. Inst. 16 (1983) 1214.
[14] S. Adachi, Optical Properties of Crystalline and Amorphous Semiconductors, first ed., Kluwer Academic Publishers, Boston/Dordrecht/London, 1999.
[15] S.H. Wemple, M. DiDomenico, Phys. Rev. B 3 (1971) 1338.
[16] A.J. Sievers, J.B. Page, Phys. Rev. B 41 (1990) 3455.
[17] D.L. Wood, J. Tauc, Phys. Rev. B 5 (1972) 3144.
[18] N.F. Mott, E.A. Davis, Electronic Process in Non-Crystalline Materials, second ed., Calendron Press, Oxford, 1979.
[19] J.E. Rowe, J.L Shay, Phys. Rev. B 3 (1971) 451.
[20] V.V. Kindyak, A.S. Kindyak, V.F. Gremenok, I.A. Victorov, Thin Solid Films 293 (1997) 75.